Journal of Asian Earth Sciences 36 (2009) 119–134

Contents lists available at ScienceDirect

Journal of Asian Earth Sciences

journal homepage: www.elsevier.com/locate/jaes

Lithospheric stress-states predicted from long-term tectonic models: Influence of rheology and possible application to Taiwan

Boris J.P. Kaus [a,c,*], Yingchun Liu [b], T.W. Becker [c], David A. Yuen [b], Yaolin Shi [d]

[a] Geophysical Fluid Dynamics, Department of Earth Sciences, NO H 9.3, Sonneggstrasse 5, ETH, 8092 Zurich, Switzerland
[b] Minnesota Supercomputer Institute, University of Minnesota, USA
[c] University of Southern California, Los Angeles, USA
[d] Laboratory of Computational Geodynamics, Graduate University of the Chinese Academy of Sciences, Beijing, China

ARTICLE INFO

Article history:
Received 5 August 2008
Received in revised form 27 February 2009
Accepted 10 April 2009

Keywords:
Lithospheric deformation
Rheology
Stress-state
Numerical modelling
Present-day tectonics

ABSTRACT

The long-term stress-state of the lithosphere results from a combination of boundary forces, surface loads and tractions from mantle flow. Here, we have employed a numerical technique which allows for the self-consistent treatment of the interaction between the lithosphere and mantle and takes into account the deformation of the free-surface. We have used this to study lithospheric dynamics in order to gain insights on the present-day conditions of stress and deformation of the lithosphere. Our numerical approach takes the observed topography and far-field plate velocities as input and computes the resultant deformation as a function of the rheological stratification.

Our model application is inspired by Taiwan tectonics. Stress data and earthquake focal mechanisms indicate that the upper crust in Taiwan may be predominantly under compression. The recent Pingtung earthquake in 12/26/2006, however, suggests that the sub-Moho mantle lithosphere under southern Taiwan may be under extension. If this earthquake indeed represents the local state of stress this raises the question as to why extension and compression can occur simultaneously in this region.

For addressing this issue we have performed a number of numerical simulations, in which we studied the effects of rheological stratification, boundary conditions and geometry on the stress-state and lithospheric dynamics. We have employed both layered viscosity models and models in which we use laboratory-based, non-Newtonian and temperature-dependent creep laws.

Results show that the rheological stratification plays an important role in lithospheric deformation. The relatively hot lithospheric thermal state in Taiwan makes it likely that part of the lower crust is relatively weak, which results in decoupling from surface-near deformation with deformation at depth. Bending of a subducting slab underneath Taiwan causes an extensional stress-state in the sub-Moho mantle lithosphere whereas the collision of the Philippine Sea plate with the Eurasian margin is responsible for a compressional state of stress in the crust. It is demonstrated that models with a weak lower crust are also in reasonable agreement with available GPS data as well as with constraints on uplift rates from long-term geodynamic modelling studies.

1. Introduction

On December 26, 2006 a Mw 6.7 earthquake occurred in Southern Taiwan (the "Pingtung earthquake sequence"), which drew attention to the tsunami risk due to earthquakes in the region. Since the focal mechanism of the deepest of the Pingtung events was rather unusual, and since the event probably occurred below the Moho, some have speculated about the geodynamic consequences of this event (Chao, 2007; Wu et al., 2009). Here, we summarize information on earthquake focal mechanisms and on the state of stress in Taiwan, with the aim to give the reader an impression on what can (and cannot yet) be inferred from available data.

1.1. State of stress in the crust and the Pingtung earthquake

The world-stress map (Reinecker et al., 2005) for Taiwan indicates that the upper crust in Taiwan is largely under compression (Fig. 1). The Pingtung event, which was the largest event in a century in that area, is composed of two major earthquakes which occurred in southern tip of Taiwan (Hengchun peninsula) within 8 minutes on December 26, 2006 (see Fig. 1b). According to the local BATS network (http://bats.earth.sinica.edu.tw/), the first event (Mw 6.7) had a centroid depth of ~41 km and had a normal fault

* Corresponding author. Address: Geophysical Fluid Dynamics, Department of Earth Sciences, NO H 9.3, Sonneggstrasse 5, 8092 Zurich, Switzerland. Tel.: +41 44 633 7539; fax: +41 44 633 1065.
E-mail address: kaus@erdw.ethz.ch (B.J.P. Kaus).

1367-9120/$ - see front matter © 2009 Elsevier Ltd. All rights reserved.
doi:10.1016/j.jseaes.2009.04.004

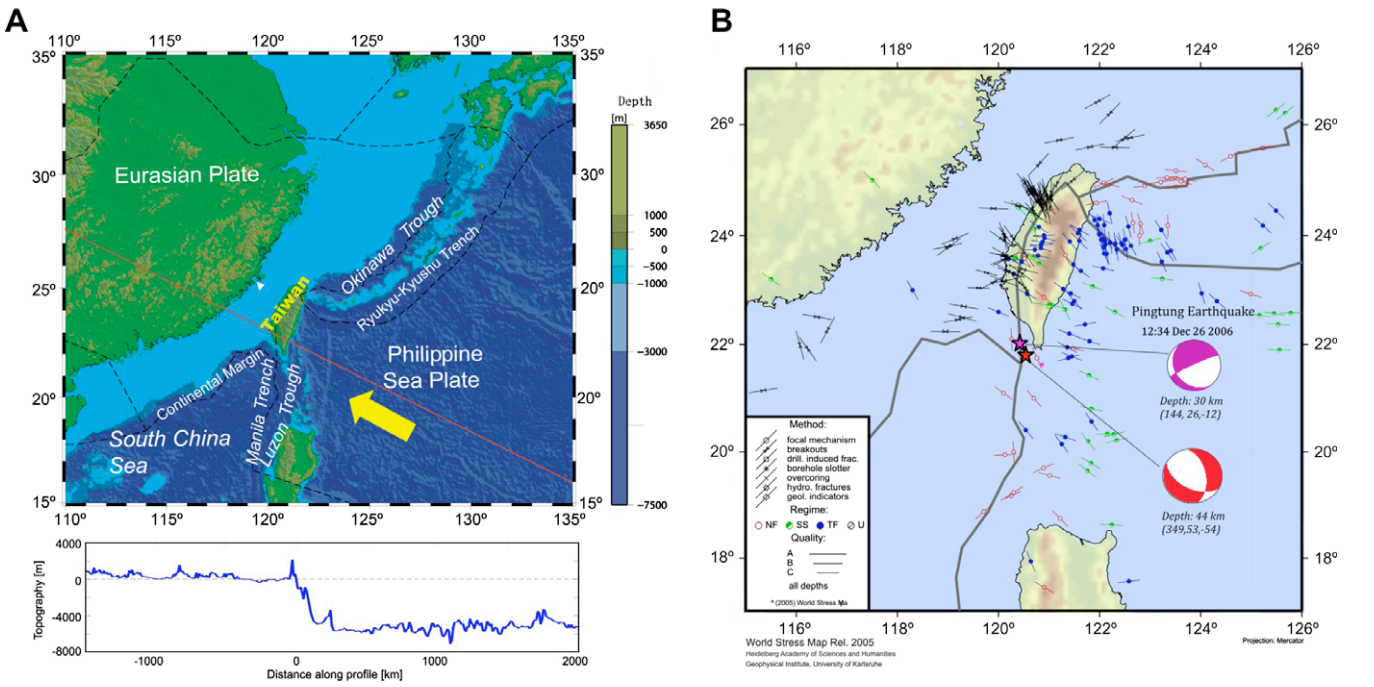

Fig. 1. (A) Topography, bathymetry and NUVEL-1A plate velocities (with respect to fixed Eurasia) of the Taiwan region. The Philippine Sea Plate (PSP) actively collides with Eurasia (EUR). Subduction of PSP underneath EUR occurs to the NE of Taiwan, whereas the EUR plate subducts in east-ward direction south of Taiwan. The red line indicates the profile along which model results are computed. (B) Stress-state of Taiwan from the world-stress map (Reinecker et al., 2005) and location and focal mechanisms of the December 26, 2006 Pingtung earthquake (using BATS data). Deformation in the Taiwanese crust is dominated by thrust and strike-slip deformation. (For interpretation of the references in colour in this figure legend, the reader is referred to the web version of this article.)

mechanism. The second event (Mw 6.5), on the other hand, had a strike-slip fault mechanism and had a higher centroid depth (30 km). A reflection seismic profile that crosses the Hengchun Peninsula (McIntosh et al., 2005) as well as a 3D velocity structure model (Kim et al., 2005), indicates that the upper crust at this location has a thickness of about 20 km and that the Moho is at a depth of around 30–35 km. The depth uncertainty for BATS CMT solutions is indicated to be in the range of 1–3 km (Kao et al., 2002). It thus appears plausible that the first Pingtung earthquake occurred in the sub-Moho mantle lithosphere, followed by a strike-slip event in the crust. A more recent study, which relocated earthquake events of the Pingtung earthquake as well as derived an improved local tomographic model of Southern Taiwan (Wu et al., 2009) confirms that the first Pingtung earthquake was a normal faulting event and suggested that this event is related to subduction. It, however, placed the second, strike-slip, event at a deeper location of ~50 km. This illustrates the sensitivity of focal depths to the local velocity model which remains incompletely understood at this stage.

1.2. Earthquake focal mechanisms throughout Taiwan

The distribution of focal mechanisms with depth is a potentially interesting dataset that, in principle, can yield insight about the local state of stress in the lithosphere. In order to do so, however, it is important to have a high precision, long duration, catalogue. The most accurate, publicly available, dataset for Taiwan is the BATS catalogue which reports Centroid Moment Tensors (CMT) from 1995–2008. Strictly speaking, CMT solutions yield information about the orientation of the strain axes and not of the stress axes. For our purposes, the differences that might exist are likely to be small (Mckenzie, 1969).

We have used earthquakes from the BATS CMT solutions (http://bats.earth.sinica.edu.tw/) with a magnitude larger than 3.5 from this dataset and sorted earthquakes according to their focal mechanisms using their rake as an indication (thrust faults: $45° < \text{rake} < 135°$; normal faults $-135° < \text{rake} < -45°$; and strike-slip $|\text{rake}| > 135°$, $-45° < |\text{rake}| < 45°$). The reported focal depth uncertainty of those solutions is 3–10 km (Kao et al., 2002). Of the 1084 earthquakes, 56 have normal, 335 thrust and 693 strike-slip fault mechanisms. A map view of earthquake distribution versus depth (Fig. 1) shows that the majority of the earthquakes occur in the upper crust (which is also dominated by strike-slip and thrust-type earthquakes). The Pingtung earthquake is one of few larger normal fault earthquakes which likely occurred beneath the Moho (note that thrust-faults and strike-slip focal mechanisms also occur at these depth).

In order to get additional insight in the earthquake distribution versus depth, we have analyzed two regions in more detail (1 and 2 in Fig. 2a). Both regions are selected to minimize artifacts from the northward subduction of the PSP plate underneath EUR. Region 1 broadly represents the continental area and Taiwan, whereas region 2 represents the colliding oceanic plate.

The depth distributions of earthquakes, sorted by focal mechanisms (and binned in 5 km bins) show that the majority of strike-slip and thrust faults occur in the upper crust, and that their number rapidly decreases with depth (Fig. 2c). Normal fault earthquakes are much rarer, but show a two-peak distribution in the continental region, which is not observed in the oceanic region, although this is not significant in a statistical sense, given the small number of earthquakes.

A plot of earthquake type and location versus depth along the topographic profile of Fig. 1 shows that the majority of earthquakes occur in the upper crust, and are of strike-slip or thrust-type. The Pingtung event occurred in a region that is otherwise dominated by strike-slip events (Fig. 2c).

1.3. Geodynamic interpretation

It is difficult to draw robust conclusions from the available dataset. Although the Pingtung event is the largest normal fault earthquake at these depths, it is surrounded by strike-slip events (as

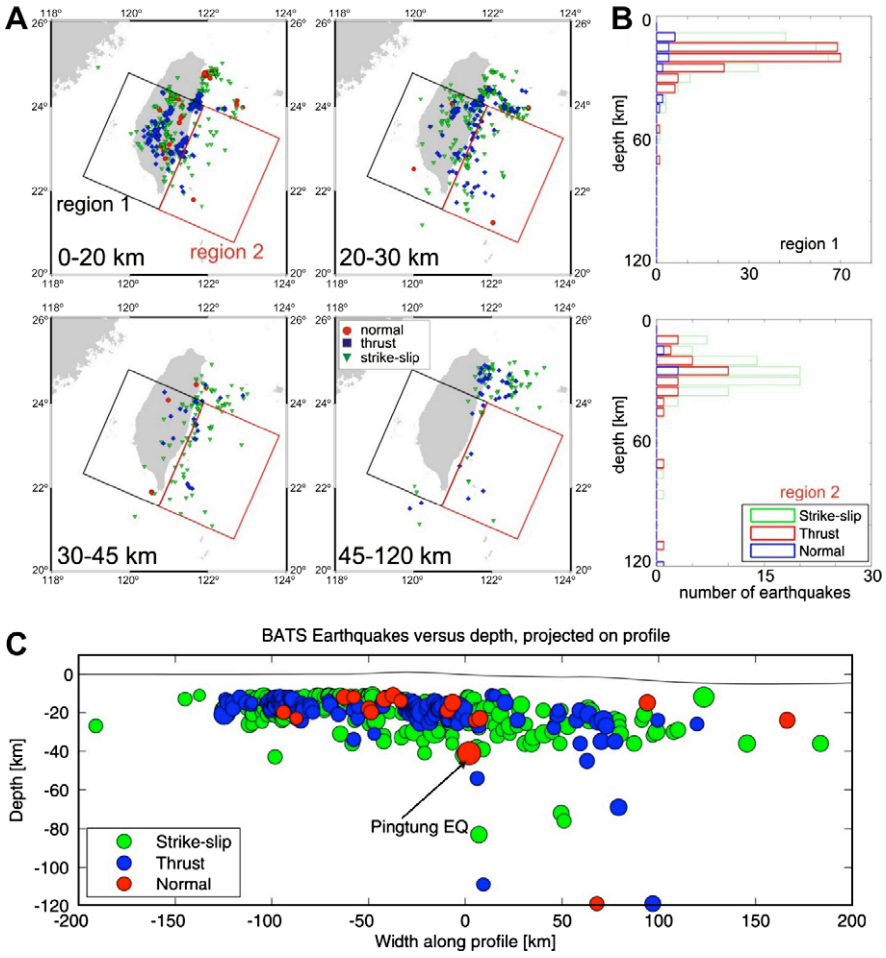

Fig. 2. (A) Distribution of earthquake type versus depth for the Taiwan region, based on the BATS catalogue from 1990–2008 (BATS CMT data is provided by the Institute of Earth Sciences, Academia Sinica, Taiwan). (B) Number of strike-slip, normal and thrust earthquakes versus depth, both for region 1 (continent) and region 2 (PSP). Note that only four normal fault earthquakes occurred in region 2. (C) Earthquake type versus depth projected from 50 km on either side of the topographic profile to the profile. The majority is of strike-slip or thrust-type and occur in the upper crust; earthquakes in the immediate vicinity of the Pingtung earthquake are of strike-slip or normal fault type.

well as a possible gap in earthquakes above the Pingtung event). The occurrence of strike-slip events is expected given the 3D deformation of Taiwan (and possible southward migration of deformation). Even when strike-slip earthquakes in the profile are not considered, however, it is difficult to judge whether there are regions in the lower lithosphere that favor one particular type of earthquakes focal mechanism. The upper crust in Taiwan above the Pingtung earthquake has significantly more earthquakes, of predominantly thrust-type. This is in agreement with data from the World-stress map and this thus suggests a compressional nature for the stress-state in the upper crust.

We thus may conjecture that there is evidence for a compressional state of stress in the Taiwanese upper crust. At deeper levels in the lithosphere, the stress-state is not inconsistent with being extensional (as suggested by the Pingtung earthquake), but more data are required to further substantiate this hypothesis.

Recently, Wu et al. (2009) relocated and reanalyzed the Pingtung earthquake sequence and concluded that the first Pingtung event is a west-dipping normal fault with a focal depth of 44 km. The second event and the largest aftershock are of strike-slip orientation.

In the remainder of this paper we will illustrate how stresses arising from long-term tectonic processes can vary as a function of lithospheric rheology. Combined with new and extended datasets on earthquake focal mechanisms, this is a potentially powerful tool that might help distinguishing various proposed geodynamical models for Taiwan, particularly because new data is expected in the future, for example through the ongoing TAIGER project (Wu and team, 2007).

We want to stress that it is not our aim to model the exact geometry in Southern Taiwan, mainly because we feel that there is currently no consensus as to what this geometry is. Partly, this stems from non-uniqueness of tomographic models, sensitivity of hypocenter locations to accurate velocity models and the possible significant three-dimensionality of the Moho. Our aim is rather to highlight the importance of variations in lithospheric rheology on the stress-state of the lithosphere as well as on the surface and mantle velocities.

The occurrence of large, intra-plate normal fault earthquakes is not unique to Taiwan, but has also been observed in other subduction zones, such as in Mexico (Singh et al., 1984) and Peru (Beck and Ruff, 1989). A global compilation of large intra-plate subduction-related earthquakes is given in Seno and Yoshida (2004), who show that many of those are down-dip tensional in nature, consistent with slab bending. Conrad et al. (2004) show that such bending-related (moderately-sized) earthquakes predominantly occur in subduction zones with weak coupling to the overriding plate. The Earth's greatest earthquakes, on the other hand, occur in compressional environments in which the coupling between subducting and overriding plate is strong, and in which the slabs are nearly completely detached from their subducting plates.

Most locations cited above, however, are related to ocean-continent subduction zones. The situation in Taiwan involves the collision of a continental margin with an overriding oceanic plate. In this case it is not entirely straightforward to predict the intra-plate state of stress and surface velocities as a function of lithospheric rheology. For this reason we here use geodynamic numerical modeling to obtain insights in the first order controls of the lithospheric state of stress.

2. Numerical modelling approach

2.1. Modelling philosophy

The state of stress of the lithosphere depends on many factors. Among them are the material properties, boundary conditions, surface loads and basal shear stress exerted by the underlying mantle circulation. In order to understand the relative importance from all of these contributions, it is vital to have numerical techniques which can treat the mantle lithosphere interaction involving both oceanic and continental lithospheres in a self-consistent manner, while taking into account the effects of topographical undulations by a free-surface boundary condition. The Taiwan region stands out as an excellent example for carrying out these kinds of numerical experiments because of its relatively young history and the interaction between the overriding oceanic Philippine plate (PSP) and a subducting Eurasian continental lithosphere (EUR) (e.g. Beyssac et al., 2007; Chai, 1972; Lallemand et al., 2001; Malavieille et al., 2002; Sibuet and Hsu, 2004).

Traditional type of lithospheric modeling has focused on its long-term evolution, over millions of years (e.g., Beaumont et al., 2001; Gerya et al., 2004; Kaus et al., 2008; Yamato et al., 2009). Here, we will instead employ a newly developed numerical method to derive insights in the present-day state of stress and deformation of the lithosphere.

We call this approach "quasi-instantaneous lithospheric modeling" (QIL), which takes the observed topography and far-field plate velocities as the input parameters and then computes the resultant deformation from variations of the rheological parameters. A similar approach has been employed by Burov et al. (1999) to study profiles through the Western Alps and more recently by Dorbath et al. (2008) to study the double seismic zone in a cross-section through the Andes. Liu and Bird (2006) used a similar approach to address the likelihood of various proposed geodynamic scenarios for southern New Zealand.

Our work is inspired by the tectonics around Taiwan, where the Philippine Sea plate collides with the Eurasian plate to form a young and active orogeny. Stress indicators such as earthquake focal mechanisms and borehole breakouts reveal that Taiwan's upper crust is primarily under compression. However, the recent Pingtung earthquake on December 26, 2006, implies that the mantle lithosphere under southern Taiwan may be in extension because of normal faulting, associated with the initial Pingtung event. This transition from compressive to extension in the stress raises the question as to why extension and compression can occur simultaneously in an overall compressive orogen.

We next describe our numerical method and governing equations. In Section 3 we describe the model setup and the numerical approach for answering some of these questions concerning the rheological stratification. In Section 4 we summarize our results and discuss future perspectives of this approach.

2.2. Numerical methodology

The deformation of rocks in the lithosphere and upper mantle can be modeled with the Boussinesq approximation, which is expressed by the following conservation equations for mass and momentum:

$$\dot{\varepsilon}_{ii} = 0, \tag{1}$$

$$-\frac{\partial P}{\partial x_i} + \frac{\partial \tau_{ij}}{\partial x_j} = \rho g_i, \tag{2}$$

where $\dot{\varepsilon}_{ij} = \frac{1}{2}\left(\frac{\partial v_i}{\partial x_j} + \frac{\partial v_j}{\partial x_i}\right)$ indicates strain rate, v_i velocity, $P = -\frac{\sigma_{ii}}{3}$ pressure, σ_{ij} stress, $\tau_{ij} = \sigma_{ij} + P$ deviatoric stress, x_i spatial coordinates (in the 2D case employed here: $x_1 = x, x_2 = z$), ρ density and g_i the gravitational acceleration (in our sign convention compressive stresses are negative). Note that the right-hand-side of Eq. (2) includes body forces which will arise if density differences exist. Thus slab-pull is automatically included if the slab has a density that is lower than the surrounding mantle.

The rheology of rocks is assumed to be visco-plastic, which is a commonly used approach in the long-term lithospheric modelling community (e.g., Braun et al., 2008; Fullsack, 1995; Moresi et al., 2007), in which case the constitutive relationship is given by

$$\dot{\varepsilon}_{ij} = \frac{1}{2\eta}\tau_{ij} + \dot{\lambda}\frac{\partial Q}{\partial \sigma_{ij}}, \tag{3}$$

where η is the effective viscosity, $\dot{\lambda}$ the plastic multiplier and Q the plastic flow potential (e.g., Moresi et al., 2007).

Rocks fail in a plastic manner if differential stresses exceed the yield stress. A commonly used, phenomenological, yield stress formulation under low temperatures is Mohr Coulomb plasticity, for which (in 2D) the yield function and plastic flow potential can be written as (e.g., Vermeer and de Borst, 1984)

$$\begin{aligned} F &= \tau^* - \sigma^* sin(\phi) - c cos(\phi), \\ Q &= \tau^* - \sigma^* sin(\psi), \end{aligned} \tag{4}$$

where $\tau^* = \sqrt{\left(\frac{\sigma_{xx}-\sigma_{zz}}{2}\right)^2 + \sigma_{xz}^2}, \sigma^* = -0.5(\sigma_{xx} + \sigma_{zz}), c$ is cohesion, ϕ friction angle, ψ the dilation angle (zero in incompressible cases). ϕ is typically 30° for dry and less for wet rocks, such as serpentine (e.g., Ranalli, 1995). Plasticity is activated only if stresses are above the yield stress:

$$\dot{\lambda} \geqslant 0, \quad F \leqslant 0, \quad \dot{\lambda}F = 0. \tag{5}$$

Conservation of energy is given by

$$\rho C_p\left(\frac{\partial T}{\partial t} + v_j\frac{\partial T}{\partial x_j}\right) = \frac{\partial}{\partial x_i}\left(k\frac{\partial T}{\partial x_i}\right) + H, \tag{6}$$

Where c_p is the specific heat capacity, k thermal conductivity and H heat production.

Density is temperature-dependent according to

$$\rho = \rho_0(1 - \alpha(T - T_{i0})), \tag{7}$$

where ρ_0 is the density at $T = T_{i0}$ (reference temperature, taken to be room temperature here), and α the thermal expansivity.

The viscosity of rocks that deform in the power law creep regime has a strain rate and temperature dependency that can be approximated as

$$\eta = \eta_0\left(\frac{\dot{\varepsilon}_{II}}{\dot{\varepsilon}_0}\right)^{\frac{1}{n}-1} exp\left(E\left(\frac{1}{T} - \frac{1}{T_0}\right)\right) \tag{8}$$

where $\dot{\varepsilon}_0, T_0$ are characteristic strain rates and temperatures respectively, E the rescaled activation energy, n the power law exponent, $\dot{\varepsilon} = \sqrt{0.5\dot{\varepsilon}_{ij}\dot{\varepsilon}_{ij}}$ the second invariant of the strain rate tensor (where the Einstein summation convention applies), and η_0 the effective viscosity at $\dot{\varepsilon}_{II} = \dot{\varepsilon}_0, T = T_0$.

Eqs. (1)–(8) are solved numerically with the recently developed finite element code MILAMIN_VEP. MILAMIN_VEP is build on top of the highly efficient, MATLAB-based, unstructured finite element code MILAMIN (Dabrowski et al., 2008) which employs high-order

elements to solve the incompressible Stokes equations with a velocity–pressure formulation (e.g., Cuvelier et al., 1986). MILAMIN_VEP is similar to a previously developed code, SloMo (Kaus et al., 2008), and employs marker techniques to track material properties and remeshing to deal with large deformations. The use of unstructured meshes as well as optimized matrix assembly techniques and fast direct solvers resulted in a considerable performance gain of MILAMIN_VEP versus SloMo. Plastic yielding is computed by decreasing viscosity locally until stresses are at the yield stress, which requires iterations since this affects local stress balance (iterations are stopped once the relative change in velocity is smaller than 10^{-3}). This way of modelling plasticity does not result in faults in a strict sense (discontinuous zones), but rather results in shear bands which are several elements in width. Such an approach, however, has been demonstrated to be relatively powerful in reproducing sand box experiments (Buiter et al., 2006) and in reproducing large offset shear zones on geological timescales (Gerya and Yuen, 2007; Lemiale et al., 2008; Moresi et al., 2003; Moresi et al., 2007).

MILAMIN_VEP has been benchmarked versus a range of analytical solutions (such as for folding and Rayleigh–Taylor instabilities, see e.g. Kaus (2005)) as well as with different numerical codes (Deubelbeiss and Kaus, 2008; Schmeling et al., 2008).

In this work, we are interested in how the *tectonic* stress-state of the lithosphere depends on the rheological stratification of the lithosphere. In order to do this, we ignore elastic effects of rheology, and assume that rheology is either purely viscous or plastic. The advantage of this approach is that the results do not depend on the initial stress-state of the lithosphere, which is difficult, or impossible, to constrain. A disadvantage is that we over-predict stress magnitudes in areas that do not fail plastically but that have a Maxwell relaxation time larger than the typical model time. In practice, this affects non-plastic model regions with an effective viscosity larger than 10^{22}–10^{23} Pa s (assuming a typical model time of 50 kyrs and elastic shear modulus of $G = 10^{10}$–10^{11} Pa). Since, in most models, there are only few such areas our approach gives a reasonable estimate of the stress-state.

In a first set of the simulations presented here, we assume viscosity and density to be constant in a specific lithospheric layer ($n = 1$, $E = 0$, $\alpha = 0$). In the second part of this work, laboratory-derived creep laws are employed as well as full coupling to the thermal evolution equation.

3. Model setup and QIL approach

Recent tomographic results and earthquake hypocenter locations indicate that it is likely that a slab is present underneath Taiwan, up to a depth of perhaps 300 km (Wang et al., 2006). This slab is likely to present a piece of Eurasian oceanic plate that is now subducted underneath the Philippine Sea Plate. Whereas the exact subduction angle is poorly constrained, a recent tomographic study as well as earthquake focal mechanisms south of Taiwan indicate that it is likely to be steep (Wang et al., 2006), consistent with a earthquakes hypocenters and a recently improved tomographic model of the Pingtung Region (Wu et al., in press). We therefore consider two scenarios: (1) a model in which the slab subducts with ~60° and (2) a model in which the slab is vertical (Fig. 3). Surface topography for the models is taken from ETOPO2 (with slight smoothening). A triangular finite element mesh is generated from the boundaries between different domains. The models are pushed with far-field velocity V_p, which is varied (with the exception of models with $V_p = 0$, which have no prescribed plate velocity). Pushing velocities are applied at a distance of 200 km's from the right side of the model box (Fig. 2). Mechanical boundary conditions are free-slip, except at the upper boundary which is completely traction-free. Thermal boundary conditions are isothermal at the lower and upper boundary and insulating at the side boundaries. A simple way to simulate large-scale mantle flow with the current approach is to leave a space between the side of the model and the oceanic plate. Alternative approaches would be to prescribe velocities at the side of the numerical domain (employed e.g. by Huismans and Beaumont, 2002), to take the details of thinning of the oceanic plate towards the mid-oceanic ridge into account (e.g., Kaus et al., 2008). The first approach might result in stress focusing at the side boundaries (if the effective viscosity varies with depth and velocity is prescribed kinematically), whereas the latter approach complicates the model setup with no obvious benefit, if velocity is prescribed kinematically. We have performed additional

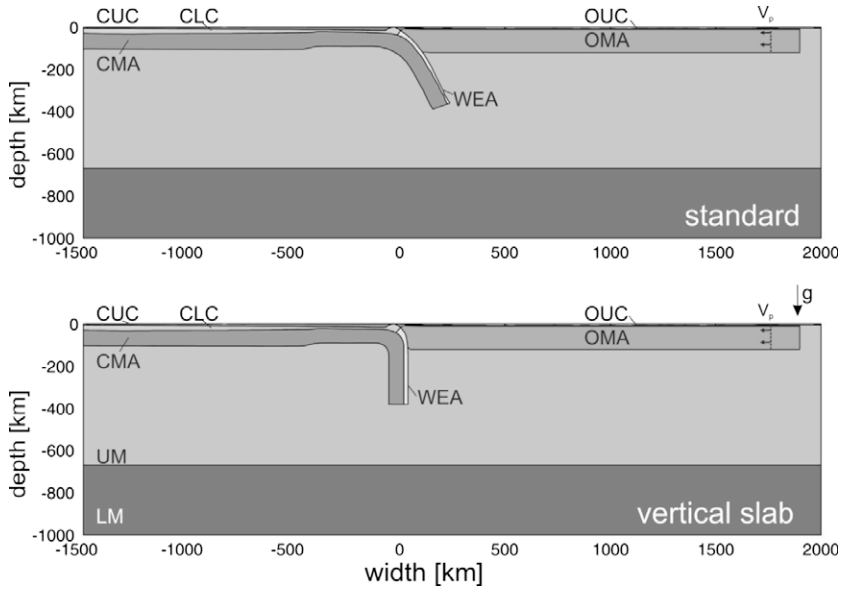

Fig. 3. Model setup for the standard and vertical slab model. CUC-continental upper crust; CLC – continental lower crust, CMA – continental mantle lithosphere; UM-upper mantle, LM – lower mantle, WEA – weak zone, OUC – oceanic upper crust, OMA – oceanic mantle lithosphere. Boundaries are free-slip, except the upper boundary, which is stress-free. Topography for the upper surface is taken from observations (Fig. 1). In some simulations, the oceanic plate is pushed with a constant, horizontal, velocity V_p. In the first set of runs, material parameters (such as density and viscosity), are constant in every layer (see Table 1 for material parameters).

numerical experiments in which no space was present between the lithosphere and the right side of the box. The results for such a kinematically prescribed far-field velocity boundary condition were very similar as the once presented here.

In most models, the effective mechanical thickness of the PSP plate is larger than the thickness of the Eurasian margin. Support for this comes from dating of sediments in oceanic drill holes, which indicate that the oceanic plate east of Taiwan could be as old as 100–120 Ma (Deschamps et al., 2000), in agreement with heat-flow measurements (Chi and Reed, 2008). We did, however, perform a number of simulations in which the thickness of the PSP plate was varied. Results (Appendix A), indicate that our conclusions are not very sensitive to the exact thickness of this plate.

The QIL approach assumes that rheology is visco-plastic, and, consequently, deformation is instantaneously related to stress. If we would have employed a free-slip upper boundary condition, it would be sufficient to compute one time step, which is common practice in global mantle flow modelling (e.g., Hager and O'Connell, 1981), and in some regional scale models of subduction zone dynamics (e.g., Billen and Gurnis, 2003; Billen et al., 2003; Vassiliou and Hager, 1988). It has however been argued that free-surface effects might be important for lithospheric-scale deformation (e.g., Royden et al., 1997) and therefore we include it in our models. Since, in this case, the starting model is typically not in perfect isostatic equilibrium, some time steps are required upon model initialization to re-establish isostatic equilibrium. The models are therefore ran forward in time until they reached 100 kyrs or until $|\Delta V_{rms}|/V_{rms} < 10^{-4}$, where V_{rms} is the average rms-velocity in the whole model domain Typically, this was achieved after a few tens of kyrs. After this time, subsequent deformation and stress patterns remain steady.

4. Results: stress states from geodynamic models

In order to obtain insight in the stresses that result from different geodynamic scenarios, we first present a number of models in which the lithosphere is divided into layers (e.g. upper crust, lower crust etc.) that each have constant material properties which do not depend on temperature (i.e. constant viscosity, density, friction angle and cohesion). The main advantage of this approach is that it minimizes the number of model parameters, which allows us to perform a systematic parameter study. An obvious shortcoming is that rock viscosity is both temperature and stress-dependent. Therefore, we will later present results of temperature-dependent simulations.

4.1. Constant viscosity cases

4.1.1. Effect of rheological layering on stress distribution

Principal stress directions, magnitude and upper-mantle flow patterns for two different end-member models are shown in Fig. 4. The standard model (Fig. 4a and c), consists of a strong (higher viscous) mantle lithosphere, a strong upper crust and a weak lower crust (see Table 1 for material parameters). The interface between subducting and overriding zone is represented by a 'weak' zone. Compressional stresses are observed in the overriding oceanic plate and in the continental upper crust. These stresses result from the indentation of the PSP oceanic lithosphere with the EUR passive continental margin. The stress pattern of the continental mantle lithosphere, on the other hand, is dominated by bending stresses, with extensional stresses just below the Moho and with compressional stresses at deeper levels. The presence of a weak lower crust effectively decouples deformation at depth from deformation in the upper crust, and allows for a situation in which the upper crust is in a state of compression, whereas the mantle lithosphere is under extension. If, the lower crust has a higher viscosity, this decoupling effect is reduced. As a result, stress magnitudes are larger whereas principal stress directions are shallower (Fig. 4b).

The simulations also show that in all cases instantaneous velocity vectors cross the subducting slab. This is in agreement with numerical and analogue models of subduction (e.g., Bellahsen et al., 2005; Enns et al., 2005; Funiciello et al., 2003; Garfunkel et al., 1986; Piromallo et al., 2006; Schmeling et al., 2008; Stegman et al., 2006).

In order to obtain insight in what controls principal stress directions and magnitudes in the mantle lithosphere, we have performed over 60 numerical simulations in which we varied the viscosities of the various layers as well as the boundary velocities while keeping all other parameters constant. In most cases, resulting stresses in the upper crust (around Taiwan) are compressional in nature. Stress levels and directions in the continental mantle lithosphere are, however, more parameter-dependent.

Fig. 5 shows a comparison of the principal stress direction and magnitude in the mantle lithosphere underneath Taiwan, for various model parameters. Increasing the density contrast between subducting slab and mantle (Fig. 5A), increasing the viscosity of the oceanic mantle lithosphere (Fig. 5B) or increasing V_{pl} (Fig. 5C), results in moderate changes of stress magnitudes, but has a negligible effect on the orientation of σ_1 (which indicates an extensional stress field in all cases). Changing the effective viscosity of the lower crust does not alter stress orientations, unless the effective viscosity of the lower crust is equal or larger than that of the continental mantle lithosphere (Fig. 5D), which results in slightly shallower principal stress directions. Stress magnitudes decrease if the coupling between continental mantle lithosphere and continental upper crust is stronger (Fig. 5D), which supports the idea that extensional stresses in the mantle lithosphere (as observed in e.g. Fig. 4) are mainly caused by slab bending (which is easier for a weak lower crust).

Increasing the effective viscosity of the continental mantle lithosphere results in a significant increase in stress magnitudes (Fig. 5E), which is consistent with the idea that extensional stresses in the mantle lithosphere are caused by bending. Maximum bending stresses occur at the top of the subducting slab and are given by $\sigma \propto \eta \frac{vh}{R^2}$, where η is the viscosity, h the thickness of the plate, v a characteristic velocity, and R the radius of curvature of the slab (e.g., Conrad and Hager, 1999). Since in our simulations changes

Table 1
Model parameters employed for the constant property models, in which material parameters are constant within each layer. Numbers in square brackets indicate standard values. Gravitational acceleration g is 9.81 ms^{-2}, plate velocity V_p was varied between 0 and 10 cm/year.

kg Pa LM	Lower mantle	3.10^{21}	3200	0	1000
CUC	Continental upper crust	10^{22}–10^{26} [10^{24}]	2750	30	20
CLC	Continental lower crust	10^{20}–10^{24} [10^{21}]	2800	30	20
CMA	Continental mantle lithosphere	10^{21}–10^{26} [10^{24}]	3210–3300 [3250]	0	1000
OUC	Oceanic upper crust	10^{22}–10^{26} [10^{25}]	2800	30	20
OMA	Oceanic mantle lithosphere	10^{21}–10^{26} [10^{23}]	3250	0	1000
WEA	Weak zone	10^{19}–10^{24} [10^{21}]	3210–3300 [3250]	30	20

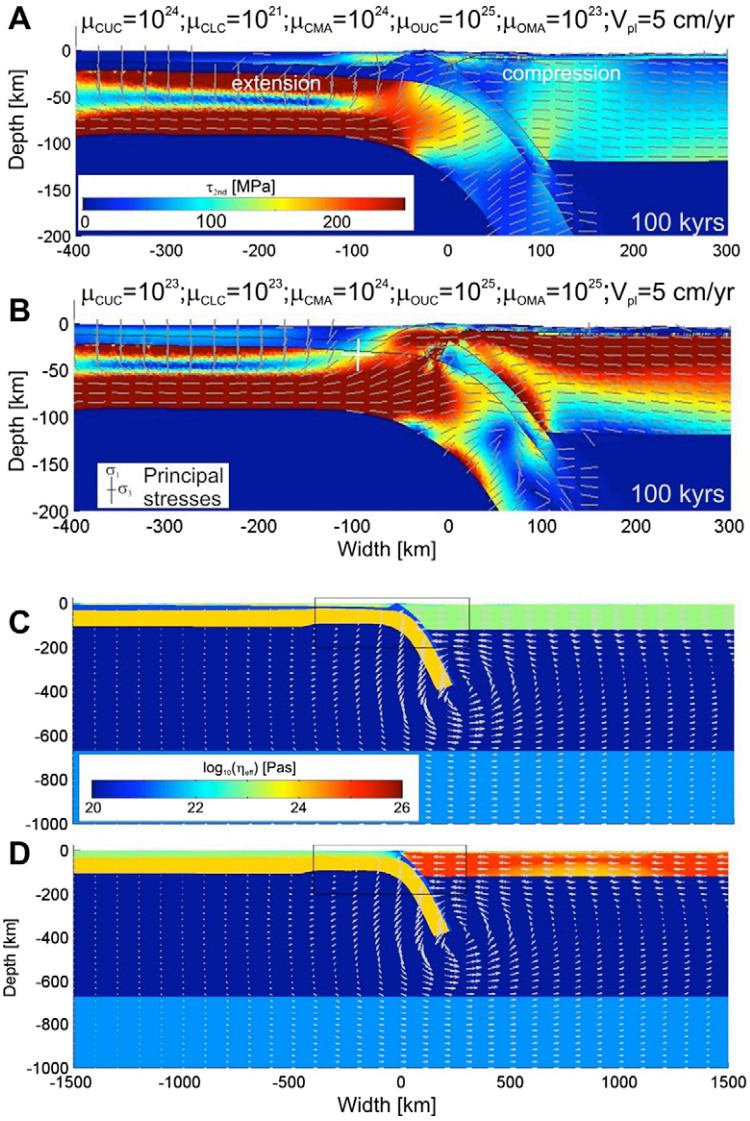

Fig. 4. Geodynamically predicted stresses (A and B) and effective viscosities with flow fields (C and D) for the standard model setup (A and C) and for a strong lower crust setup (B and D). (A) Stress distribution in a zoomed-in part of the standard model (setup shown in Fig. 4a). Colors indicate the second invariant of the deviatoric stress tensor. Gray crosses indicate principal stress directions and are shown at locations with $\tau^{2nd} > 10$ MPa (which is taken as a typical stress-drop during an earthquake). Extensional regions have vertical bars. (B) The same but for a model with a strong lower crust. (C) Upper mantle flow field and effective viscosities for the standard model in (A). (D) The same but for the model shown in B.

in viscosity are the dominating parameter, bending predicts a linear relationship between stress magnitudes and effective viscosity. Numerical simulations confirm this for mantle lithosphere values larger than 10^{23} Pa s (inset in Fig. 5E). We emphasize that stresses in the mantle lithosphere are compressional rather than extensional for effective viscosities of the mantle lithosphere less than 10^{23} Pa s.

Increasing the viscosity of the weak zone induces a switch from a high stress/extensional regime to a lower stress/compressional regime for effective viscosities larger than 10^{22} Pa s, thus highlighting the importance of coupling between subducting and overriding plate (Fig. 5F). These results are consistent with earlier work on subduction zone dynamics (e.g., Billen and Gurnis, 2003; Buiter et al., 2001).

To further illustrate the effects of changing model parameters on lithospheric stress-state, we show a number of end-member modes on Fig. 6. If the mantle lithosphere is weak, stresses are concentrated in the crust (Fig. 6B). If the lower crust is strong, rather than weak extensional bending stresses occur in the lower crust rather than in sub-Moho regions, which in turn affects stress states in the crust (Fig. 6C). If coupling between subducting and overriding plates is strong ($\mu_{WEA} \sim 10^{23}$ Pa s), the overriding PSP plate and the continental mantle lithosphere form a through-going stress guide, that has predominantly compressive stresses (Fig. 6D).

If the Pingtung earthquakes were indeed indicative for the stress-state in Taiwan (see Section 2), one may conclude that the geodynamic models presented here favor cases in which plate coupling is weak, the viscosity of the lower crust is small, but the sub-Moho mantle lithosphere has sufficiently large effective viscosities to cause significant, bending-related, extensional stresses to develop.

4.1.2. Effects of model geometry

Tomographic data of Taiwan indicate that the dip of the subducting slab underneath Taiwan might change from vertical in the center of Taiwan to steeply eastward dipping in Southern Taiwan (Wang et al., 2006). In order to understand the sensitivity of the model results on changes in geometry, we have performed a

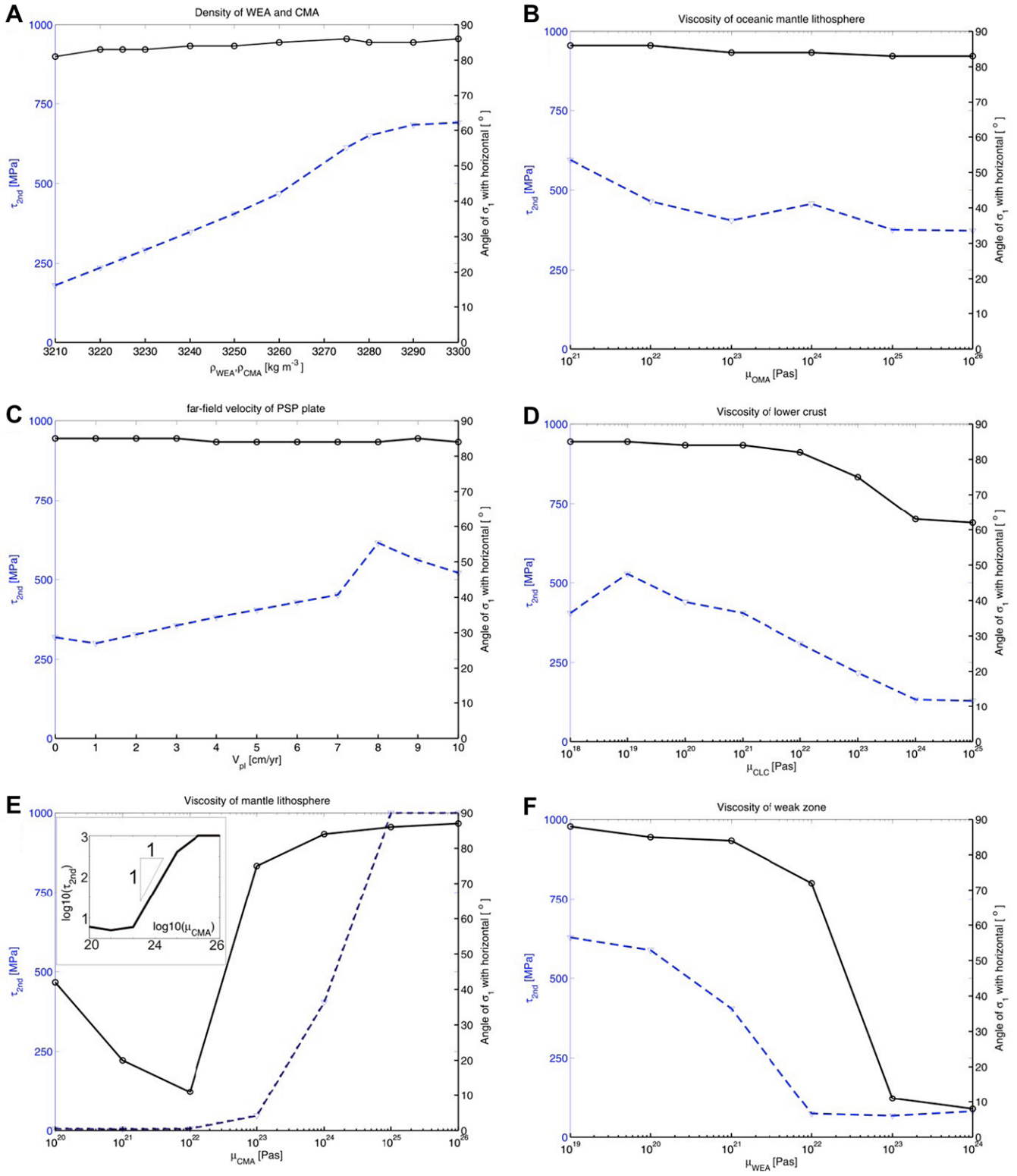

Fig. 5. Effect of various model parameters on the orientation and magnitude of principal stresses in the mantle lithosphere at location [width = −100 km, depth = −35 km] (see Fig. 5b for location). Lines with circles indicate the angle of σ_1 with horizontal (>45 extensional and <45 compressional); dashed lines indicate stress magnitudes. (A) Effect of changing the density of the initially subducting slab, (B) effect of changing the viscosity of the oceanic mantle, (C) effect of far-field velocity, (D) effect of lower crustal strength. Changes in the viscosity of the upper continental and oceanic crust do not affect stress magnitudes and orientations and results are therefore not shown here, (E) effect of changing the viscosity of the mantle lithosphere (note that compression occurs if the viscosity is smaller than 10^{23} Pa s, although stresses are significantly reduced in this case). Inset shows the same on a logarithmic scale, from which it follows that stresses scale nearly linearly with viscosity for viscosity values larger than 10^{23} Pa s, (F) effect of the coupling between subducting and overriding plates: strong coupling results in compression.

number of experiments in which we compare stress states and magnitudes for two different geometries. Results indicate that although small changes in stress magnitudes occur, the overall patterns are similar (Fig. 7), which can also be seen in simulations in which the thickness of the Philippine Sea plate was changed (Fig. A1).

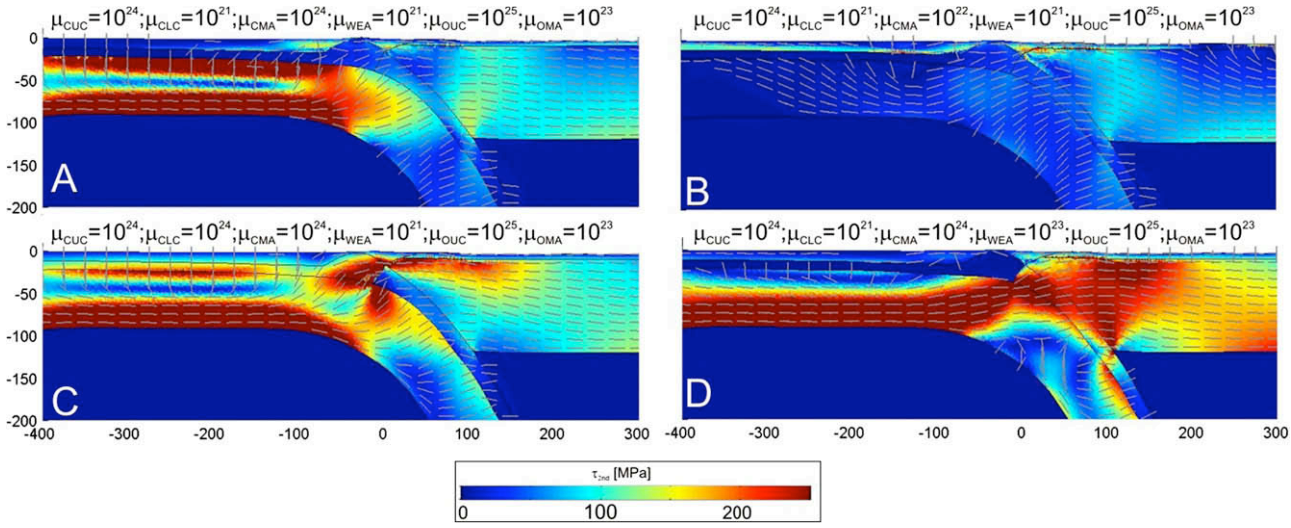

Fig. 6. Instantaneous solutions illustrating the types of stresses that are obtained by changing model parameters (from the study summarized in Fig. 6). (A) Standard model. (B) Weak continental mantle lithosphere (10^{22} Pa s). (C) Strong lower crust (10^{24} Pa s). (D) Strong coupling between subducting and overriding plate (channel viscosity 10^{23} Pa s).

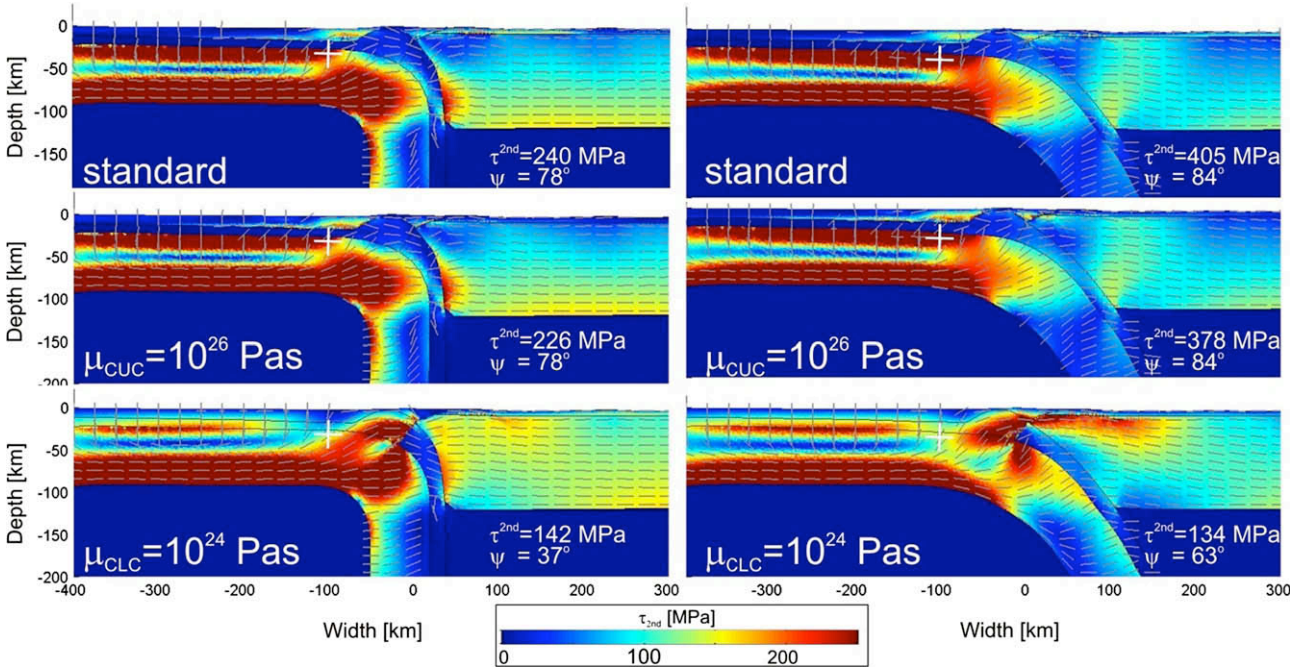

Fig. 7. Effect of model geometry on stress patterns, with vertical slab models (left) and inclined slab models (right column), for the standard rheology (upper row), for a stronger upper crust (middle row) and for a stronger lower crust (lower row). Stress magnitudes and principal stress direction at location (−100, −35) km are also indicated (white cross on plots). Stress patterns are similar for both model geometries. Stress magnitudes are typically somewhat smaller for vertical slabs, which is mainly caused by a horizontal shift in regions with large stresses.

4.1.3. Effect of overriding plate velocity on surface velocity and induced mantle flow

The relationship between far-field plate velocity, mantle flow patterns and surface velocity is illustrated on Fig. 8, for various model parameters.

Results show that large-scale mantle flow is induced even if no far-field plate velocity is applied (Fig. 8A). In this case, the oceanic plate moves at a constant velocity of ~1 cm/yr toward the trench (Fig. 8E), driven by the negative buoyancy of the small sliver of oceanic lithosphere underneath Taiwan. The continental lithosphere, however, also moves toward the trench, in disagreement with GPS data for the Taiwan region (Yu et al., 1997). Observed velocities of the PSP are of the order of 8 cm/yr. These modelling results thus imply that mantle drag caused by a subducting slab underneath Taiwan is responsible for a small part of this velocity only. The remaining part is likely caused by northward subduction of the Philippine Sea plate underneath the EUR plate, toroidal mantle flow underneath Taiwan, or by flow due to other subduction zones in the region.

Since our model setup is two-dimensional, this effect is best modeled by applying a far-field velocity boundary condition. Results show that the plate velocity of the PSP plate remains constant over the length of the plate, as long as applied plate velocities do not exceed 5 cm/yr. Far-field plate velocities of 10 cm/yr induce a

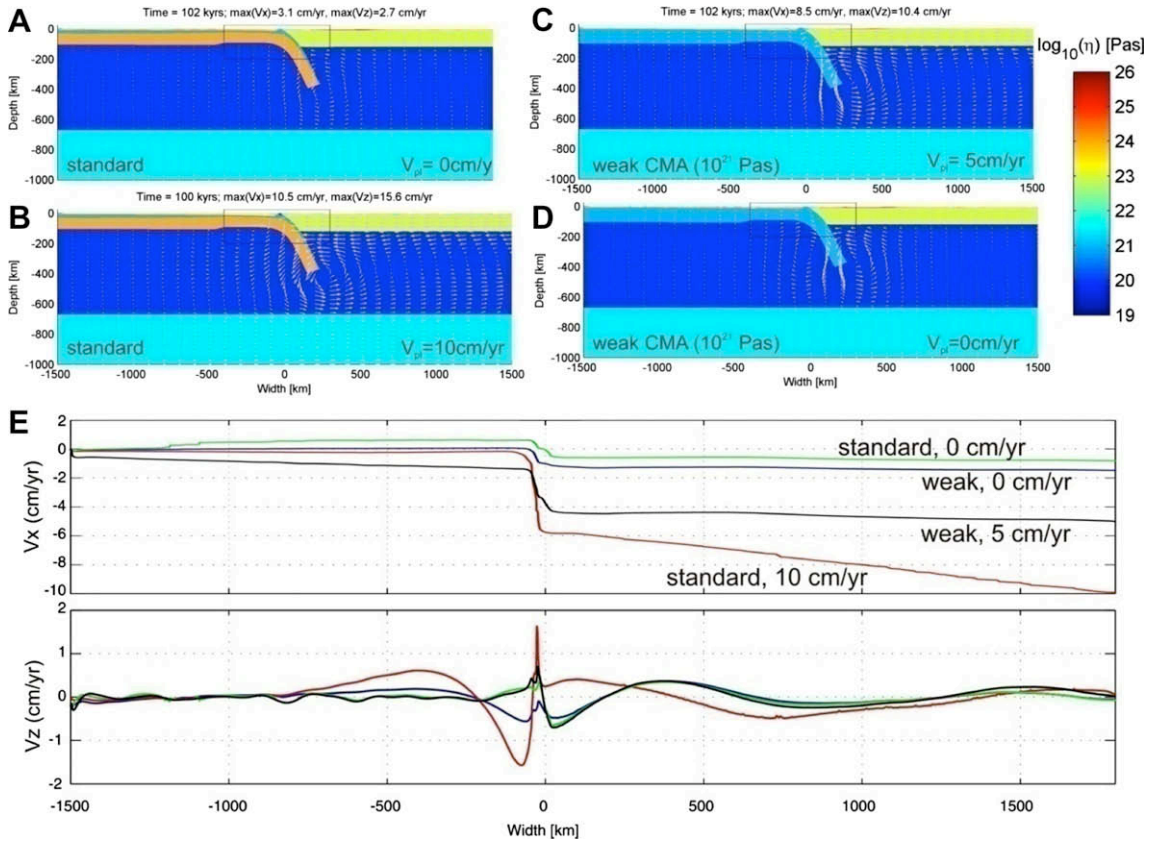

Fig. 8. Effect of far-field plate velocity (V_{pl}) and rheology of the mantle lithosphere on large-scale mantle flow. (A–D) Effective viscosity and large-scale mantle flow for standard models and weak-mantle lithosphere models with various far-field velocities. (E) Horizontal and vertical velocity at the surface of the models shown in A–D. Note that the oceanic plate moves with an almost constant velocity (i.e. deforms in a plate-like mode), except in the case of V_{pl} = 10 cm/yr, where a gradient in surface velocity occurs. A weak-mantle lithosphere, in absence of far-field velocities, results in a sinking of the slab similar to a Rayleigh–Taylor instability, in which both oceanic and continental plates are dragged towards the subduction zone.

gradient in the surface velocity of the overriding PSP plate (Fig. 8C and E). All models predict a relatively sharp gradient in horizontal surface velocities around Taiwan, which is accompanied by positive uplift rates, unless the mantle lithosphere is very weak (Fig. 8E).

4.1.4. Surface velocities and comparison with GPS data

It is interesting to know whether it is theoretically possible to distinguish various model scenarios on the basis of surface observables, such as GPS velocity. For this reason, we have compared model results with GPS data (Yu et al., 1997). Since the models are two-dimensional, we use stations that are within 50 km on either side of our modeled profile (Fig. 1). The velocity data was subsequently rotated and projected onto the profile. The GPS data is referenced with respect to a station to the west of Taiwan. Since China is fixed in our numerical setup, the GPS data can be compared with surface velocity from the numerical models.

Results show that the agreement between modeled and observed horizontal surface velocities is reasonable in most cases (Fig. 9). A model with strong coupling between EUR and PSP plates clearly disagrees with observations; the standard model with V_p = 10 cm/yr results in velocity gradients in the oceanic plate (unlike the real Earth). The scatter in the data, however, is too large to make clear distinction between any of the other models on the basis of horizontal surface velocities alone (Fig. 9A). The calculated vertical velocities would in theory be more convincing (Fig. 9B). These data are, unfortunately, more difficult to obtain. Some independent constraints on exhumation rates in Southern Taiwan come from fission track data, which indicate cooling rates of the order of 130–330 K per million year. Making the (uncertain) assumption that the geotherm is in steady-state and around 30 K/km, this translates into exhumation rates of 0.4–1.0 cm/yr, which is in agreement with the results from long-term geodynamic models for Taiwan (Kaus et al., 2008; Yamato et al., 2009).

An obvious problem with the comparison of GPS data and model results is that the geodynamic models give an estimate of the *long-term* velocities, whereas GPS data might contain a significant amount of co-seismic motion and interseismic locking. Previous models, however, gave encouraging results of comparisons between GPS velocities and (thin-sheet type) geodynamic models on a orogenic scale (e.g., Cook and Royden, 2008; Flesch et al., 2000).

4.2. Temperature-dependent viscosities

The results in the previous section demonstrate that an extensional stress field in the upper mantle can occur due to bending of slab underneath Taiwan, as long as the lower crust in Taiwan is weak. An obvious shortcoming of those models, however, is that they ignore nonlinear effects as well as the temperature-dependence of viscosity. For this reason, we have performed a series of additional experiments in which we incorporate laboratory-based creep laws. A major complication with performing such experiments is our lack of knowledge of the temperature distribution with depth underneath Taiwan, as well as the considerable uncertainty of rheological laws (e.g., Burov, 2003). Surface heatflow is rather high, and increases from around 80-100 mW/m^2 in the Western Foreland up to 150–200 mW/m^2 in the Central Range (Barr

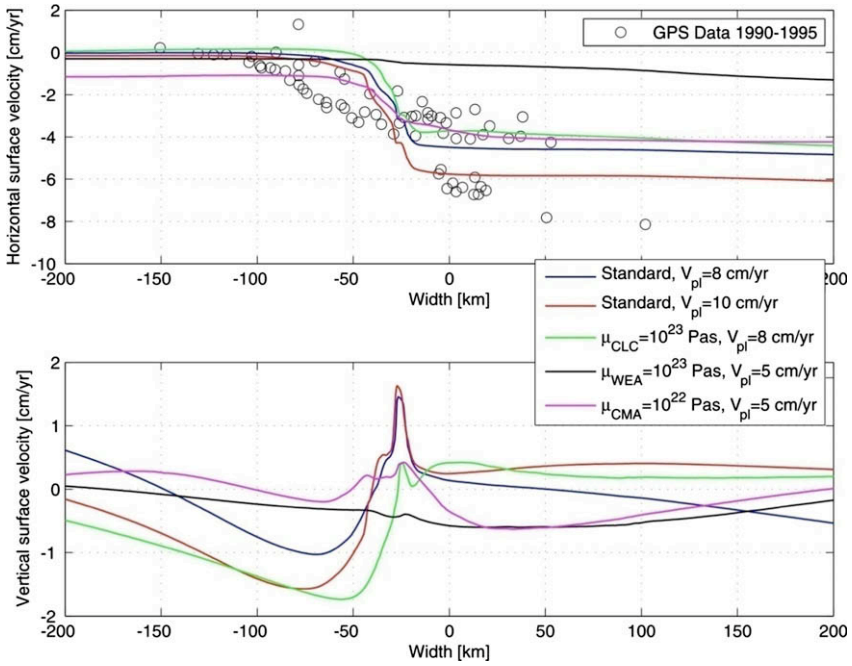

Fig. 9. Horizontal (a) and vertical (b) surface velocity around Taiwan for various model parameters (for constant property models). Also shown are GPS data that have been 50 km wide band on both sides of our profile, which were subsequently projected onto our profile to allow a fair comparison between models and data. Models with strong coupling between overriding and subducting plate lead to a poor data fit. Distinguishing between the other models is difficult on the basis of horizontal surface velocities only. Vertical velocities are more variable and are generally larger in the presence of a weak lower crust.

and Dahlen, 1989; Chi and Reed, 2008). In addition to technical challenges in obtaining accurate heat-flow measurements in rapidly eroding mountainbelts, it is unclear to which extent the measured (surface) values are representative for the geotherm throughout the whole lithosphere. Factors such as the distribution of radioactive elements in the crust (and non-steadiness of the geotherm) might have a considerable effect.

An additional complication in using temperature-dependent creep laws is the uncertainty of the creep laws itself. Changes in mineralogy or water content result in orders of magnitude differences in effective viscosity (e.g., Ranalli, 1995). Moreover, the creep laws are obtained on small samples and involve extrapolations over many orders of magnitude to natural length and time scales.

Thus, the uncertainties in employing laboratory data are quite large. Since we are here mainly concerned with the overall effects of rheological stratification on stress-state, we restrict our analysis to two, highly simplified, thermal structures for which we employ both 'weak' and 'strong' creep law end-members for the rheology of various lithospheric layers. Rheological parameters are given in Table 2, and the thermal setup on Fig. 10. The thermal structure consists of an oceanic Philippine Sea Plate with a thermal age of 70 Myrs and an EUR continental margin with a thermal age of 40 Myrs (note that radioactive heat producing layers are taken into account in the computation of the initial geotherm – see Table 2). The difference in the two thermal models is the initial temperature structure of the subducting part of EUR plate. The 'normal' model employs a temperature distribution from a cooling plate model with an age of 35 Myrs, using only temperatures below a depth of 10 km. The 'hot' model, on the other hand, takes the temperature profile at $x = -100$ km and $z < -17$ km as slab temperature. This results in a larger temperature at the top of the slab. Temperatures are set in such a

Table 2
Model parameters employed for the temperature-dependent simulations. $\dot{\varepsilon}_0 = 10^{-15} s^{-1}, T_0 = 600\ ^\circ C$. Numbers in brackets refer to the following references: (1) Dry olivine (Chopra and Paterson, 1984), (2) Wet quartzite (Ranalli, 1995), (3) Dry quartzite (Ranalli, 1995), (4) Diabase (Carter and Tsenn, 1987), (5) Mafic granulite/undried piktoweini granulite (Wilks and Carter, 1990), (6) Wet olivine (Hirth and Kohlstedt, 1996).

Parameter	Symbol	Units	UM	LM	CUC	CLC	CMA	WEA	OUC	OMA
Density (at 273 K)	ρ_0	kg m^{-3}	3200	3200	2750	2800	3200	3200	2800	3200
Thermal expansivity	α	K^{-1}	3×10^{-5}	3×10^{-5}	3×10^{-5}	3×10^{-5}	3×10^{-5}	3×10^{-5}	3×10^{-5}	3×10^{-5}
Reference viscosity	η_0	Pa s	6.6×10^{24} (1)	10^{23}	6.2×10^{19} (2) 3.8×10^{20} (3)	4.7×10^{21} (4) 3.6×10^{22} (5)	6.6×10^{24} (1) 2.43×10^{23} (6)	10^{21}	6.6×10^{24} (1)	6.6×10^{24} (1)
Powerlaw exponent	n		3 (1)	1	2.3 (2) 2.4 (3)	3.05 (4) 4.2 (5)	3 (1) 3.5 (6)	1	3 (1)	3 (1)
Temperature-dependency	E	K^{-1}	2.1×10^4 (1)	0	7.8×10^3 (2) 8.1×10^3 (3)	1.1×10^4 (4) (5) 1.27×10^4	2.1×10^4 (1) (6) 1.8×10^4	0	2.1×10^4 (1)	2.1×10^4 (1)
Heat capacity	c_p	J kg^{-1} K^{-1}	1000	1000	1000	1000	1000	1000	1000	1000
Thermal conductivity	k	W m^{-1} K^{-1}	3.5	3.5	3.5	3.5	3.5	3.5	3.5	3.5
Cohesion	c	MPa	1000	1000	20	20	1000	20	20	1000
Friction angle	ϕ	$^\circ$	0	0	30	30	0	30	30	0
Radioactive heat	H	W m^{-3}	0	0	10^{-6}	10^{-6}	0	0	0	0

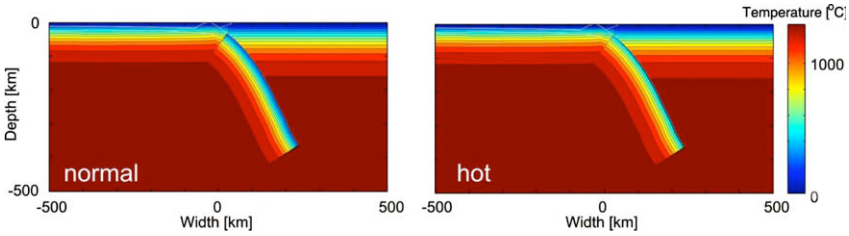

Fig. 10. Thermal setup for temperature-dependent simulations.

manner that the 1300° isotherm of the subducting slab is continuous with that of the upper plate. This results in an (artificial) discontinuity at the top of the slab. Since this part of the slab is predominantly located in the weak subduction channel, it has little effect on the dynamics of the lithosphere as can also be seen by the continuity of sub-Moho stresses (Fig. 11). In Kaus et al. (2008) we present a compilation of both 'strong' and 'weak' crustal rheologies together with 'hot' and 'cold' estimates of the geotherm. The results of that compilation indicate that in all cases one expects the lower crust underneath Taiwan to be weak. These results are consistent with 2D thermal models presented in Zhou et al. (2003) and with 2D thermo-mechanical models presented in Yamato et al. (2009) as well as here, which indicates that even 'cold' thermal structures will results in a weak lower crust.

Simulations with a strong upper crust, a strong mantle lithosphere and a weak lower crust yield a layered lithospheric stress-state with compression in the upper parts of the crust and extensional stresses in the mantle lithosphere, irrespective

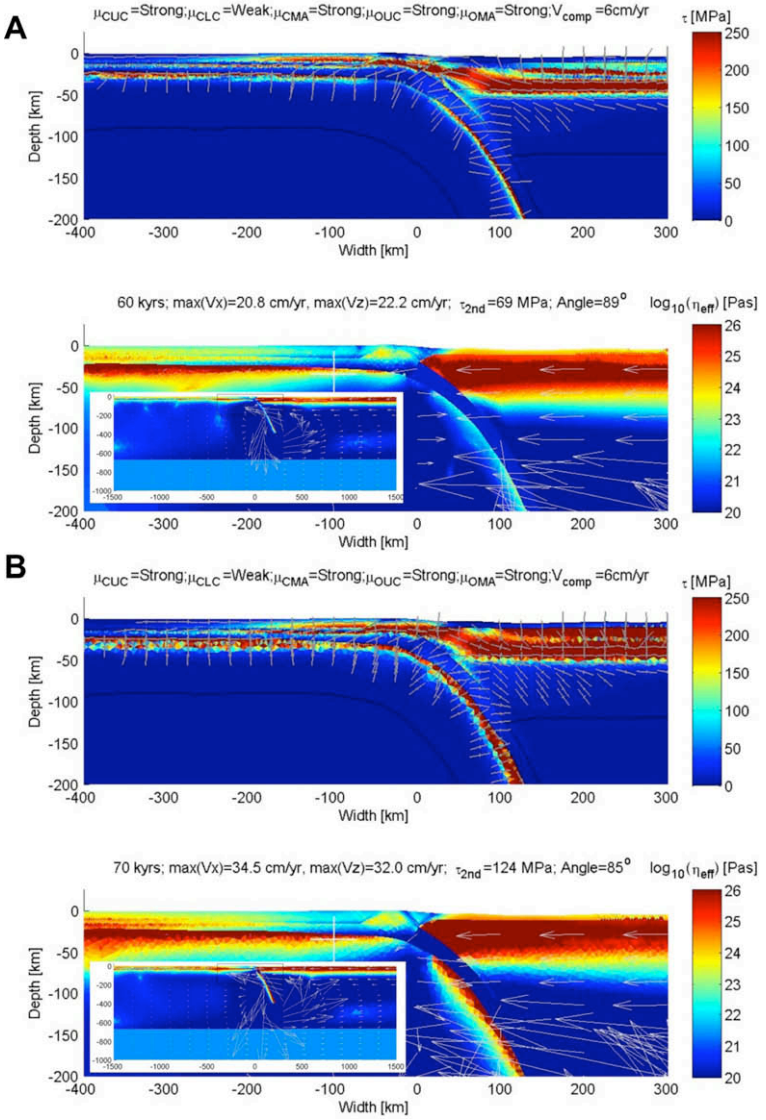

Fig. 11. Results for cases with a temperature-dependent viscosity and a vertical slab, for (A) a 'hot' and (B) a 'normal' thermal case. The temperature-dependence and nonlinearity of rheology weakens the slab significantly and causes it to 'drip-off' (see velocity patterns in inset), despite the fact that a dry olivine rheology is employed for the mantle. In both cases, compressional stress states occur in the upper crust and extensional stresses occur beneath the continental Moho. Note that the lower crust underneath Taiwan is weak in both cases.

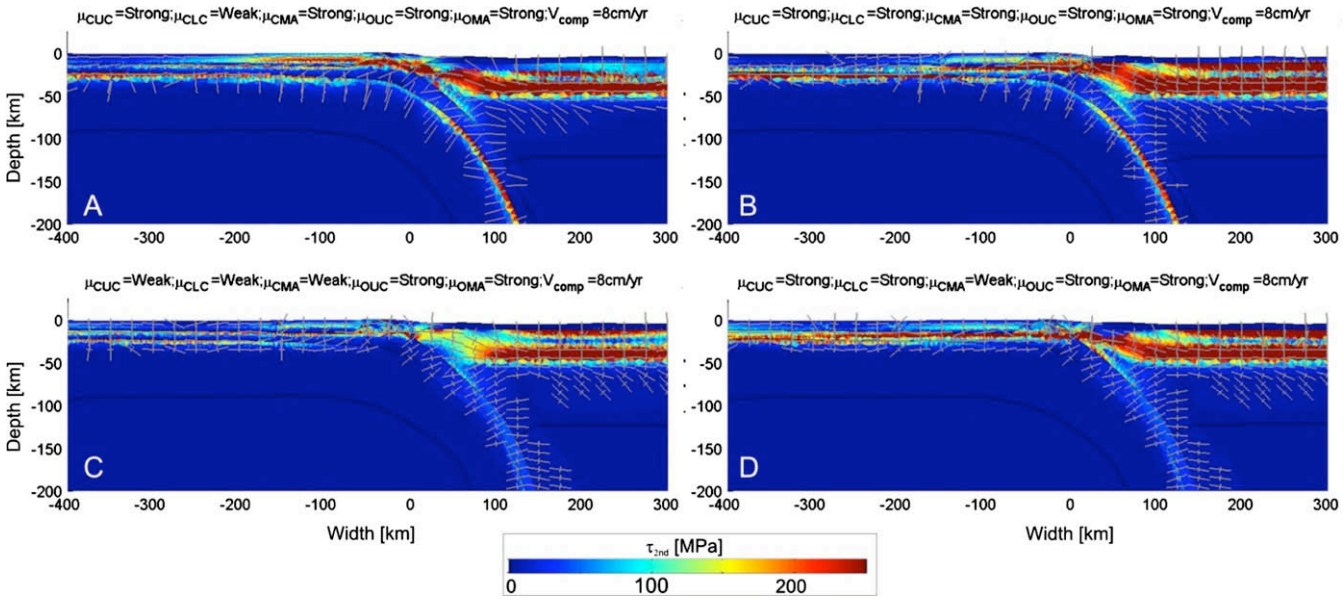

Fig. 12. Results of temperature-dependent simulations, with a 'hot' setup. (A) Far-field plate velocity 8 cm/yr. (B) Strong rather than weak continental lower crust rheology (note that minimum effective viscosities of the lower crust underneath Taiwan are on the order of 10^{21} Pa s and thus still relatively small). (C) Weak upper and lower crust and weak mantle lithosphere. (D) Weak mantle lithosphere. Cases, in which a compressional upper crust coexists with an extensional stress-state in the mantle lithosphere require a strong mantle lithosphere, as well as a weak channel in the lower crust.

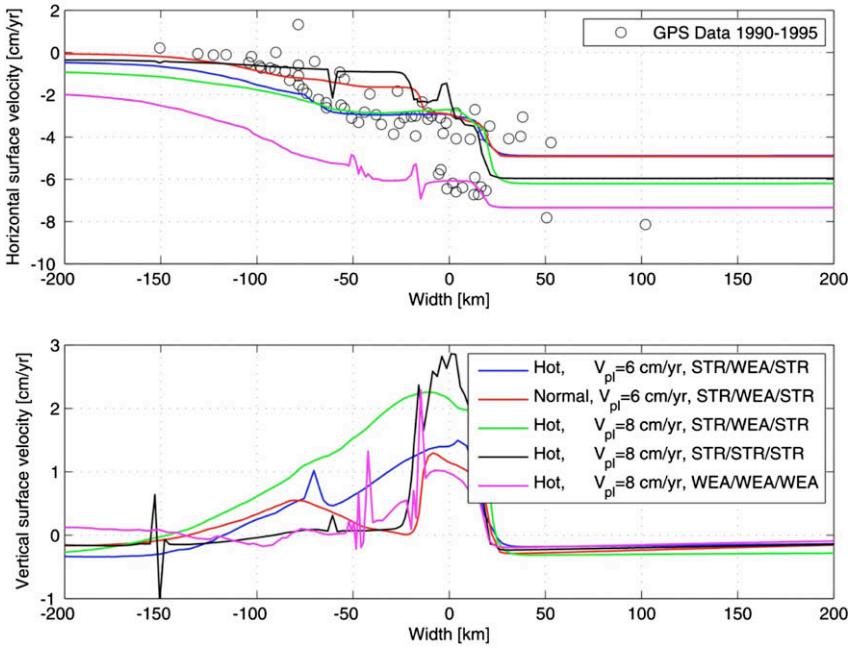

Fig. 13. Surface velocities from temperature-dependent models in Figs. 12 and 13, as well as GPS data. Compared with constant viscosity models (Fig. 10), horizontal surface velocity changes over a wider area. Discrete jumps (related to "quasi" fault zones) are more pronounced. Models with a strong mantle lithosphere appear to fit data better.

of the thermal state (Fig. 11). These results are in general agreement with constant viscosity simulations (e.g., Fig. 4), with the difference that flow velocities in the mantle are significantly larger than in constant viscosity runs. Good agreement exists between 'hot' and 'normal' setups, although normal setups, expectedly, have larger differential stresses in the mantle lithosphere. Simulations in which the rheological parameters of the continental lithosphere were varied (Fig. 12) show that the mantle lithosphere should have sufficient strength to develop an extensional stress-state, in agreement with our analysis of constant viscosity simulations (Fig. 5).

A comparison of horizontal and vertical surface velocities of various models with GPS velocities (Fig. 13) underscores our earlier findings that models with a weak lower crust and a strong mantle lithosphere are most consistent with the data.

5. Discussion and conclusions

In this study, we have employed two-dimensional lithospheric-scale models to obtain some insights into the effects of rheological stratification on the lithospheric stress-state. The quasi-instantaneous-lithosphere (QIL) modelling approach uses geodynamic

numerical models that are typically employed to address lithospheric deformation on a million years timescale. Instead of addressing such timescales, we here restrict the analysis to the *recent* tectonic state of stress of the lithosphere. A key advantage of the QIL approach is that a wider parameter space can be addressed, since it is computationally cheaper per run (each run requires a few hours on a single CPU, instead of days or weeks for million year timescale lithospheric models). Moreover, an attempt can be made to compare the estimated stress-state with the distribution of earthquakes as well as surface strain rates with constraints such as GPS velocities (with the caveats mentioned above).

Here, we have applied the models to Taiwan, where a recent normal fault earthquake (the Pingtung earthquake) beneath the Moho was followed by a strike-slip/thrust event at shallower depth. At this point, existing EQ focal mechanism catalogues do not (yet) allow judging whether this is a statistically significant observation. If confirmed, however, it might be an indication that the regional state of stress in the mantle lithosphere underneath Taiwan is extensional, whereas the state of stress in the crust is predominantly compressional. This would raise the interesting geodynamic question how one can obtain such contrasting stress states in an active compressional orogeny.

To obtain insights in this question, we ran a large number of numerical models in which various lithospheric layers either had constant or temperature-dependent material properties. The models showed that an extensional stress-state at depth can be explained by bending of a subducting plate underneath Taiwan, combined with the presence of a weak lower crustal channel. The temperature-dependent models indicate that it is likely that such a weak channel exists, due to the expected hot state of the Taiwanese lithosphere. At the same time, however, the mantle lithosphere should not be too weak, since otherwise stress states are compressional. Modeled surface velocities are in reasonable agreement with horizontal velocities obtained from GPS measurements, and seem to rule out models with either a very weak mantle lithosphere, or with a strong coupling between overriding and subducting plate.

Model predictions show that vertical surface velocities are slightly more sensitive to the rheological stratification of the lithosphere. More accurate observational constraints on the distribution of vertical motion in Taiwan (e.g. by analyzing the evolution of sedimentary basins), will thus likely help to refine the models presented here.

All temperature-dependent simulations performed here indicate that large (>20 cm/yr) mantle flow velocities occur in the mantle. This effect can be attributed to the nonlinear dependency of viscosity on strain rate, combined with relatively hot thermal state of the lithosphere, and will result in a rapid steepening of the slab underneath Taiwan. Tomographic images indeed indicate that the slab underneath central Taiwan is close to vertical, whereas it is steeply inclined in southern Taiwan (Wang et al., 2006). This is consistent with the generally accepted view that collision in Taiwan initiated in the North and progressed southward (Suppe, 1984). In principle, the significant flow velocities in the mantle should cause seismic anisotropy at depth (Rau et al., 2000), and are thus testable predictions (although three-dimensional effects might play a significant role as well, and global scale-flow should be taken into account in such calculations).

Our results are consistent with lithospheric-scale thermomechanical modelling studies that addressed the evolution of Taiwan on a Myrs timescale (Kaus et al., 2008; Yamato et al., 2009). These studies pointed out that the combination of rapid erosion, a relatively weak lower crust, and an overall compressional deformation field results in the formation of a young orogeny that shares many features with observational constraints from Taiwan (Yamato et al., 2009). As explained in Kaus et al. (2008), the rapid exhumation phase of crustal rocks as inferred from thermochronological dating, is difficult to explain unless an erosion-enhanced crustal-scale doming instability occurs.

The stress-state of Taiwan has consequences for the tsunami potential and hazard. If the stress of Taiwan is indeed predominantly compressional in the upper crust and extensional in the mantle lithosphere, we would expect predominantly normal fault earthquakes in sub-Moho regions, which are likely to cause little surface deformation (as was the case with the Pingtung Earthquake). More hazard comes from earthquakes in the upper crust, in particular ones in the western side of Taiwan, were our models predict a compressional state of stress of significant magnitude (e.g. Fig. 11).

Lastly, Taiwan is located in a complex, three-dimensional, geodynamic setting whereas our models are restricted to a two-dimensional analysis. We believe that, despite the simplifications, our models yield important insights. However, three-dimensional models are required to obtain a more complete picture, in particular in the Northern parts of Taiwan.

Acknowledgements

Work in this proposal has partly been supported by Swiss Science Foundation, grant SNF 200021-119841/1 and the IIR grant to the VLAB by the National Science Foundation. We thank Lapo Boschi for helpful discussions.

Appendix A

We performed a number of additional simulations in which the thickness of the PSP plate was changed from 120 km, to 40 km. Results (Fig. A1), support the idea that changes in the thickness of the PSP plate are of second order importance compared to changes in lithospheric rheology (e.g., Fig. 6).

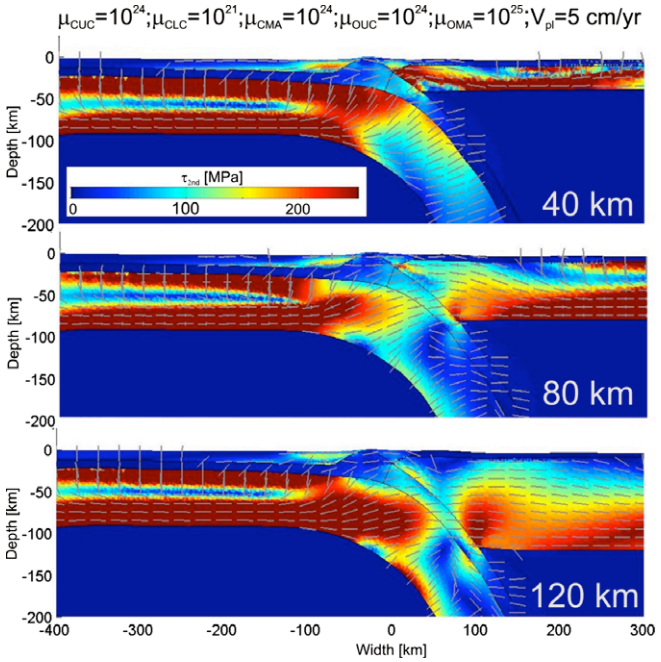

Fig. A1. Effect of varying the thickness of the PSP plate from 40 km to 120 km. All results are shown after 100 kyrs. The increased horizontal motion causes changes in the stresses of the subducting slab, but the effect is minor, compared to the effect of changing the rheology of the lower crust.

References

Barr, T.D., Dahlen, F.A., 1989. Brittle frictional mountain building – 2. Thermal structure and heat budget. Journal of Geophysical Research 94, 3923–3947.

Beaumont, C., Jamieson, R.A., Nguyen, M.H., Lee, B., 2001. Himalayan tectonics explained by extrusion of a low-viscosity crustal channel coupled to focused surface denudation. Nature 414 (6865), 738–742.

Beck, S.L., Ruff, L.J., 1989. Great earthquakes and subduction along the Peru Trench. Physics of the Earth and Planetary Interiors 57 (3–4), 199–224.

Bellahsen, N., Faccenna, C., Funiciello, F., 2005. Dynamics of subduction and plate motion in laboratory experiments: insights into the "plate tectonics" behavior of the Earth. Journal of Geophysical Research-Solid Earth 110 (B1).

Beyssac, O. et al., 2007. Late Cenozoic metamorphic evolution and exhumation of Taiwan. Tectonics 26 (TC6001). doi:10.1029/2006TC002064.

Billen, M.I., Gurnis, M., 2003. Comparison of dynamic flow models for the Central Aleutian and Tonga–Kermadec subduction zones. Geochemistry Geophysics Geosystems 4. doi:10.1029/2001gc000295.

Billen, M.I., Gurnis, M., Simons, M., 2003. Multiscale dynamics of the Tonga–Kermadec subduction zone. Geophysical Journal International 153 (2), 359–388.

Braun, J. et al., 2008. DOUAR: a new three-dimensional creeping flow numerical model for the solution of geological problems. Physics of the Earth and Planetary Interiors 171 (1–4), 76–91.

Buiter, S.J.H. et al., 2006. The numerical sandbox: comparison of model results for a shortening and an extension experiment. In: Buiter, S.J.H., Schreurs, G. (Eds.), Analogue and Numerical Modelling of Crustal-Scale Processes. Geological Society of London Special Publications, Geological Society of London, pp. 29–64.

Buiter, S.J.H., Govers, R., Wortel, M.J.R., 2001. A modelling study of vertical surface displacements at convergent plate margins. Geophysical Journal International 147 (2), 415–427.

Burov, E., Podladchkov, Y., Grandjean, G., Burg, J.P., 1999. Thermo-mechanical approach to validation of deep crustal and lithospheric structures inferred from multidisciplinary data: application to the Western and Northern Alps. Terra Nova 11 (2–3), 124–131.

Burov, E.B., 2003. The upper crust is softer than dry quartzite. Tectonophysics 361 (3–4), 321–326.

Carter, N.L., Tsenn, M.C., 1987. Flow properties of continental lithosphere. Tectonophysics 136, 27–63.

Chai, B.H.T., 1972. Structure and tectonic evolution of Taiwan. American Journal of Science 272, 389–422.

Chao, B.F., 2007. Taiwan shaken by an uncommon earthquake. Eos 88 (1), 2.

Chi, W.C., Reed, R.P., 2008. Evolution of shallow, crustal thermal structure from subduction to collision: an example from Taiwan. GSA Bulletin 120 (5–6), 679–690.

Chopra, P.N., Paterson, M.S., 1984. The role of water in the deformation of dunite. Journal of Geophysical Research 89, 7861–7876.

Conrad, C.P., Bilek, S., Lithgow-Bertelloni, C., 2004. Great earthquakes and slab pull: interaction between seismic coupling and plate-slab coupling. Earth and Planetary Science Letters 218 (1–2), 109–122.

Conrad, C.P., Hager, B.H., 1999. Effects of plate bending and fault strength at subduction zones on plate dynamics. Journal of Geophysical Research 104, 17551–17571.

Cook, K.L., Royden, L., 2008. The role of crustal strength variations in shaping orogenic plateaus, with application to Tibet. Journal of Geophysical Research 113 (B08407). doi:10.1029/2007JB005457.

Cuvelier, C., Segal, A., van Steemhoven, A.A., 1986. Finite element methods and Navier–Stokes equations. Mathematics and its Applications. Reidel Publishing Company, Dordrecht. 483 pp.

Dabrowski, M., Krotkiewski, M., Schmid, D.W., 2008. MILAMIN: MATLAB-based FEM solver for large problems. Geochemistry Geophysics Geosystems. doi:10.1029/2007GC001719.

Deschamps, A., Monie, P., Lallemand, S., Hsu, S.-K., Yeh, K.Y., 2000. Evidence for Early Cretaceous oceanic crust trapped in the Philippine Sea Plate. Earth and Planetary Science Letters 179 (3–4), 503–516.

Deubelbeiss, Y., Kaus, B.J.P., 2008. Comparison of Eulerian and Lagrangian numerical techniques for the Stokes equations in the presence of strongly varying viscosity. Physics of the Earth and Planetary Interiors 171 (1–4), 92–111.

Dorbath, C., Gerbault, M., Carlier, G., Guiraud, M., 2008. Double seismic zone of the Nazca Plate in northern Chile: high-resolution velocity structure, petrological implications, and thermomechanical modeling. Geochemistry Geophysics Geosystems 9 (Q07006). doi:10.1029/2008GC002020.

Enns, A., Becker, T.W., Schmeling, H., 2005. The dynamics of subduction and trench migration for viscosity stratification. Geophysical Journal International 160 (2), 761–775.

Flesch, L.M., Holt, W.E., Haines, A.J., Shen-Tu, B.M., 2000. Dynamics of the Pacific-North American plate boundary in the western United States. Science 287 (5454), 834–836.

Fullsack, P., 1995. An arbitrary Lagrangian–Eulerian formulation for creeping flows and its application in tectonic models. Geophysical Journal International 120 (1), 1–23.

Funiciello, F., Morra, G., Regenauer-Lieb, K., Giardini, D., 2003. Dynamics of retreating slabs (Part 1): insights from 2D numerical experiments. Journal of Geophysical Research 108 (B4), 2206. doi:10.1029/2001JB000898.

Garfunkel, Z., Anderson, D.L., Schubert, G., 1986. Mantle circulation and lateral migration of subducting slabs. Journal of Geophysical Research 91, 7205–7223.

Gerya, T.V., Yuen, D.A., 2007. Robust characteristics method for modelling multiphase visco-elasto-plastic thermo-mechanical problems. Physics of the Earth and Planetary Interiors 163 (1–4), 83–105.

Gerya, T.V., Yuen, D.A., Maresch, W.V., 2004. Thermomechanical modelling of slab detachment. Earth and Planetary Science Letters 226 (1–2), 101–116.

Hager, B.H., O'Connell, R.J., 1981. A simple global model of large-scale flow in the Earth's mantle. Journal of Geophysical Research 86, 4843–4867.

Hirth, G., Kohlstedt, D.L., 1996. Water in the oceanic upper mantle: implications for rheology, melt extraction and the evolution of the lithosphere. Earth and Planetary Science Letters 144, 93–108.

Huismans, R.S., Beaumont, C., 2002. Asymmetric lithospheric extension: the role of frictional plastic strain softening inferred from numerical experiments. Geology 30 (3), 211–214.

Kao, H., Liu, Y.-H., Liang, W.-T., Chen, W.-P., 2002. Source parameters of regional earthquakes in Taiwan: 1999–2000 Including the Chi-Chi earthquake sequence. TAO 13 (3), 279–298.

Kaus, B.J.P., 2005. Modeling approaches to geodynamic processes. Ph.D. Thesis, Swiss Federal Institute of Technology, Zurich, 256 pp.

Kaus, B.J.P., Steedman, C.E., Becker, T.W., 2008. From passive continental margin to mountain belt: insights from analytical and numerical models and application to Taiwan. Physics of the Earth and Planetary Interiors 171 (1–4), 235–251.

Kim, K.H. et al., 2005. Three-dimensional V–P and V–S structural models associated with the active subduction and collision tectonics in the Taiwan region. Geophysical Journal International 162 (1), 204–220.

Lallemand, S., Font, Y., Bijwaard, H., Kao, M., 2001. New insights on 3D plate interactions near Taiwan from tomography and tectonic implications. Tectonophysics 335, 229–253.

Lemiale, V., Muehlhaus, H.B., Moresi, L., 2008. Shear banding analysis of plastic models formulated for incompressible viscous flows. Physics of the Earth and Planetary Interiors 171 (1–4), 177–186.

Liu, Z., Bird, P., 2006. Two-dimensional and three-dimensional finite element modelling of mantle processes beneath central South Island, New Zealand. Geophysical Journal International 165 (3), 1003–1028.

Malavieille, J. et al., 2002. Arc-continent collision in Taiwan: new marine observations and tectonic evolution. In: Byrne, T., Liu, C.S. (Eds.), Geology and Geophysics of an Arc-Continent Collision. Spec. Pap. Geol. Soc. Am., pp. 187–211.

McIntosh, K. et al., 2005. Crustal-scale seismic profiles across Taiwan and the Western Philippine Sea. Tectonophysics 401 (1–2), 23–54.

Mckenzie, D.P., 1969. Relation between fault plane solutions for earthquakes and directions of principal stresses. Bulletin of the Seismological Society of America 59 (2), 591–601.

Moresi, L., Dufour, F., Muhlhaus, H.-B., 2003. A Lagrangian integration point finite element method for large deformation modeling of viscoelastic geomaterials. Journal of Computational Physics 184, 476–497.

Moresi, L. et al., 2007. Computational approaches to studying non-linear dynamics of the crust and mantle. Physics of the Earth and Planetary Interiors 163, 69–82.

Piromallo, C., Becker, T.W., Funiciello, F., Faccenna, C., 2006. Three-dimensional instantaneous mantle flow induced by subduction. Geophysical Research Letters 33 (8).

Ranalli, G., 1995. Rheology of the Earth. Chapman & Hall, London. 413 pp.

Rau, R.J., Liang, W.T., Kao, H., Huang, B.S., 2000. Shear wave anisotropy beneath the Taiwan orogen. Earth and Planetary Science Letters 177 (3–4), 177–192.

Reinecker, J., Heidbach, O., Tingay, M., Sperner, B., Müller, B., 2005. The 2005 Release of the World-Stress Map (<www.world-stress-map.org>).

Royden, L.H. et al., 1997. Surface deformation and lower crustal flow in Eastern Tibet. Science 276, 788–790.

Schmeling, H. et al., 2008. A benchmark comparison of spontaneous subduction models: towards a free surface. Physics of the Earth and Planetary Interiors 171 (1–4), 198–223.

Seno, T., Yoshida, M., 2004. Where and why do large shallow intraslab earthquakes occur? Physics of the Earth and Planetary Interiors 141 (3), 183–206.

Sibuet, J.-C., Hsu, S.-K., 2004. How was Taiwan created? Tectonophysics 379, 159–181.

Singh, S.K., Dominguez, T., Castro, R., Rodriguez, M., 1984. P-waveform of large, shallow earthquakes along the Mexican subduction zone. Bulletin of the Seismological Society of America 74 (6), 2135–2156.

Stegman, D.R., Freeman, J., Schellart, W.P., Moresi, L., May, D., 2006. Influence of trench width on subduction hinge retreat rates in 3D models of slab rollback. Geochemistry Geophysics Geosystems 7.

Suppe, J., 1984. Kinematics of arc-continent collision, flipping of subduction, and back-arc spreading near Taiwan. Geological Society of China 6, 21–34.

Vassiliou, M.S., Hager, B.H., 1988. Subduction zone earthquakes and stress in slabs. Pure and Applied Geophysics 128 (3–4), 547–624.

Vermeer, P., de Borst, R., 1984. Non-associated plasticity for soils. Concrete and Rock 29, 1–65.

Wang, Z., Zhao, D.P., Wang, J., Kao, H., 2006. Tomographic evidence for the Eurasian lithosphere subducting beneath south Taiwan. Geophysical Research Letters 33 (18). doi:10.1029/2006GL027166.

Wilks, K.R., Carter, N.L., 1990. Rheology of some continental lower crustal rocks. Tectonophysics 182, 57–77.

Wu, F.T., team, U.T.T., 2007. TAIGER (TAiwan Integrated GEodynamics Research) project for testing models of Taiwan orogeny. Geophysical Research Abstracts 9, 02135.

Wu, Y.-M. et al., in press. Relocation of the 2006 Pingtung earthquake sequence and seismotectonics in Southern Taiwan. Tectonophysics.

Wu, Y.-M. et al., 2009. Relocation of the 2006 Pingtung earthquake sequence and seismotectonics in Southern Taiwan. Tectonophysics. doi:10.1016/j.tecto.2008.12.001.

Yamato, P., Mouthereau, F., Burov, E., 2009. Taiwan mountain building: insight from 2D thermo-mechanical modeling of a rheologically-stratified lithosphere. Geophysical Journal International 176 (1), 307–326.

Yu, S.-B., Chen, H.-Y., Kuo, L.-C., 1997. Velocity field of GPS stations in the Taiwan area. Tectonophysics 274, 41–59.

Zhou, D., Yu, H.-S., Xu, H.-H., Shi, X.-B., Chou, Y.-W., 2003. Modeling of thermo-rheological structure of lithosphere under the foreland basin and mountain belt of Taiwan. Tectonophysics 374, 115–134.